INTERNATIONAL JOURNAL FOR NUMERICAL METHODS IN FLUIDS
Int. J. Numer. Meth. Fluids 2005; **47**:1061–1067
Published online 24 January 2005 in Wiley InterScience (www.interscience.wiley.com). DOI: 10.1002/fld.854

High-resolution simulation of inviscid flow in general domains

Oskar Hall, Hans Joachim Schroll*,† and Fredrik Svensson‡

Centre for Mathematical Sciences, Lund University, Box 118, SE-221 00 Lund, Sweden

SUMMARY

In this paper, a high-resolution finite volume method for calculating solutions to a hyperbolic conservation law is presented. The method works in two space dimensions on general domains and uses curvilinear meshes. A non-trivial estimation of gradients needed for the reconstructions is presented. The paper contains examples of numerical solutions of the Euler gas dynamics equations. Copyright © 2005 John Wiley & Sons, Ltd.

KEY WORDS: conservation law; hyperbolic reconstruction; high-resolution finite volume scheme; curvilinear mesh

INTRODUCTION

Inviscid flows are modelled by hyperbolic conservation laws. In numerical computations, 'conservation' is simulated in computational cells; this is the concept of finite volume (FV) schemes. FV-schemes approximate local averages in these cells, and these averages are determined cell wise by the flux balance across the cell boundaries. To achieve a reasonable accuracy of the solution, some reconstruction of the unknown profile of the flux in each cell is needed. In Reference [1], Marquina presented a hyperbolic ansatz for the reconstruction, which is extended to work on domains of general shapes in two space dimensions. These general domains yield non-Cartesian, quadrilateral meshes, so the method presented here handles these cases.

The ansatz for the reconstruction of fluxes reads

$$r(x, y) = a + \frac{b}{x - x_0 + c} + \frac{d}{y - y_0 + e} \tag{1}$$

*Correspondence to: Hans Joachim Schroll, Centre for Mathematical Sciences, Lund University, Box 118, SE-221 00 Lund, Sweden.
†E-mail: achim.schroll@na.lu.se
‡E-mail: fredrik.svensson@na.lu.se

Contract/grant sponsor: European network HYKE; contract/grant number: HPRN-CT-2002-00282

Received 27 April 2004
Revised 17 August 2004
Accepted 10 September 2004

where (x_0, y_0) is the cell centre and the remaining five parameters are determined such that the cell average a is preserved, and certain directional derivatives along all four edges are prescribed (see Reference [2]). Thus, gradients need to be determined from the known cell averages. This is established as follows.

NUMERICAL GRADIENTS

Based on discrete data $f(p_i)$ available in the centre $p_i \in C_i \subset \mathbb{R}^2$ of quadrilateral cells, the goal is to determine the gradient $\nabla f(\bar{p})$ on a given boundary point $\bar{p} \in \partial C_i$. By a linear combination of data from neighbouring cells

$$\sum_i \mu_i f(p_i) = f_x(\bar{p}) + \mathcal{O}(\Delta^2) \tag{2}$$

the x-derivative is approximated up to second order, for example. Here, Δ is the size of a cell side. To eliminate the leading order term in the expansion

$$\begin{aligned} f(x,y) = f(\bar{p}) &+ f_x(\bar{p})(x-\bar{x}) + f_y(\bar{p})(y-\bar{y}) \\ &+ \tfrac{1}{2} f_{xx}(\bar{p})(x-\bar{x})^2 + f_{xy}(\bar{p})(x-\bar{x})(y-\bar{y}) \\ &+ \tfrac{1}{2} f_{yy}(\bar{p})(y-\bar{y})^2 + \mathcal{O}(\|p-\bar{p}\|^3) \end{aligned}$$

clearly, the coefficients have to sum up to zero

$$\sum_i \mu_i = 0 \tag{3}$$

Moreover, to approximate $f_x(\bar{p})$ and to eliminate the remaining four error terms the conditions are

$$\begin{aligned} \text{first order:} \quad & \textstyle\sum \mu_i (x_i - \bar{x}) = 1, \quad \sum \mu_i (y_i - \bar{y}) = 0 \\ \text{second order:} \quad & \textstyle\sum \mu_i (x_i - \bar{x})^2 = \sum \mu_i (x_i - \bar{x})(y_i - \bar{y}) = \sum \mu_i (y_i - \bar{y})^2 = 0 \end{aligned} \tag{4}$$

In the present work, these six order conditions are satisfied using a six-point stencil as shown in Figure 1. Given the mesh, the coefficients μ_i are numerically computed from the linear system $\mathbf{A}\mu = \mathbf{b}$ representing the order conditions (3) and (4) and stored during the rest of the computation.

There is some freedom in choosing the six-point stencil; however, one has to make sure that $\mathbf{A}$ is regular throughout the mesh. In the Cartesian case, the stencil selected above leads to a regular system for μ with unique solution $\mu = (0, -1/2h, 1/2h, 1/2h, -1/2h, 0)^{\mathrm{T}}$ for all positive step sizes h. Formula (2) reduces to an average of two central differences in this case. This argument shows also that for moderately non-Cartesian meshes, formula (2) is still uniquely determined.

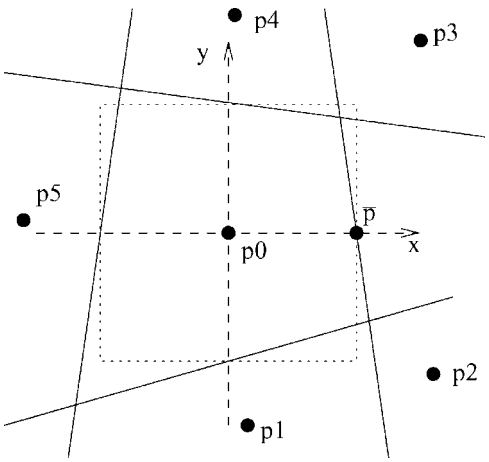

Figure 1. Chosen stencil.

HYPERBOLIC RECONSTRUCTION A LA MARQUINA

Given averages of an unknown function f

$$v_j = \frac{1}{\Delta x}\int_{x_{j-1/2}}^{x_{j+1/2}} f(\xi)\,\mathrm{d}\xi$$

on an equidistant mesh in one space dimension, the following three conditions

$$d_{j-1/2} = \frac{v_j - v_{j-1}}{\Delta x} = r'(x_{j-1/2}) \tag{5}$$

$$v_j = \frac{1}{\Delta x}\int_{j-1/2}^{j+1/2} r(\xi)\,\mathrm{d}\xi \tag{6}$$

$$d_{j+1/2} = \frac{v_{j+1} - v_j}{\Delta x} = r'(x_{j+1/2}) \tag{7}$$

define a third-order accurate reconstruction r within the actual cell $C_j = [x_{j-1/2}, x_{j+1/2})$ such that

$$|r(\xi) - f(\xi)| = \mathcal{O}(\Delta x^3), \quad \xi \in C_j$$

See Reference [2] or [3].

Marquina [1] established a hyperbolic reconstruction based on this principle

$$r_j^{\mathrm{M}}(x) = a_j + \frac{b_j}{x - x_j + c_j} \tag{8}$$

Whenever the given data are monotonic ($d_{j+1/2}d_{j-1/2} > 0$), there is a unique (monotonic) hyperbola satisfying (5)–(7). Otherwise, in transition cells, the lateral derivative with largest

absolute value is replaced by the other one multiplied by Δx^2. In this way, the order of accuracy drops to two in transition cells.

This local hyperbolic reconstruction is quite successful in 1D, see References [1, 3–5]. Here, we present an extension to 2D in the following way.

Consider a generic cell with central point p_0, see Figure 1. Imagine a local co-ordinate system such that the corners of the cell appear in different quadrants. In this situation, the unknown quantity is reconstructed by the bi-hyperbolic ansatz (1) along the local co-ordinate system. For simplicity, we perform two 1D-reconstructions in x- and y-direction, respectively. Partial derivatives in the boundary points $\bar{p}$ on all four edges are approximated as described in the previous section. Then it is straightforward to apply Marquina's 1D algorithm in both co-ordinate directions. The result is a bi-hyperbolic reconstruction (1), which is third-order accurate along *both* co-ordinate directions. Note, however, that third-order accuracy cannot be expected throughout the whole generic non-Cartesian cell. This is due to the following reason: the 1D-reconstructions preserve the 1D-averages along both co-ordinate axes. Therefore, the given average within the 2D computational cell equals the average of reconstruction (1) within the dotted rectangle in Figure 1, which differs from the cell average of (1). In rectangular cells of course, this effect is irrelevant and full third order is achieved. Otherwise, the average could be fixed by adjusting the constant a in (1). The integration is tedious, however, and numerical results do not justify the effort.

FLUX BALANCING AND TIME INTEGRATION

The dynamics of the flow is governed by the flux balance along the boundary of computational cells $C_i \subset \Omega \subset \mathbb{R}^2$,

$$\frac{\mathrm{d}}{\mathrm{d}t}\int_{C_i} U(t,z)\,\mathrm{d}z + \int_{\partial C_i} F(U(t,z))\cdot\mathbf{n}\,\mathrm{d}S = 0$$

Here, $z = (x, y) \in \mathbb{R}^2$ and $\mathbf{n}$ denotes the outward normal along the boundary ∂C_i.

In a numerical simulation on quadrilateral cells, the normal flux $F(U)\cdot\mathbf{n}$ needs to be integrated along all four edges of each cell. To determine the flux on the interface, we apply a flux splitting formula, which in the case of the Euler equations is van Leer's splitting [6]. The partial fluxes $F^{\pm}$ are reconstructed according to the previous section, and the normal flux $F(U)\cdot\mathbf{n}$ is integrated along the edge using a standard quadrature rule. Finally, to advance the solution in time, the flux balance is integrated using the third order non-linear SSP-RK scheme in Reference [7], Section 4.1.

NUMERICAL RESULTS

Shock–bubble interaction

Initially investigated experimentally by Haas and Sturtevant [8], the shock–bubble experiment, where a shock wave in air impinges on a bubble of helium has drawn the attention for numerical tests (Figure 2). The gases are assumed to be perfect and governed by Euler's equations for a 2D, compressible gas flow. To describe the two different components of

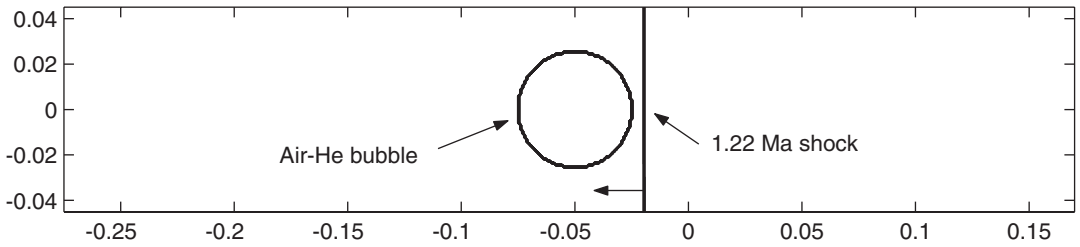

Figure 2. Initial configuration for the shock-bubble experiment.

Table I. Mean velocities for the shock–bubble experiment.

	V_s	V_r	V_t	$V_{ui(1)}$	$V_{ui(2)}$	V_{di}	V_j
Bi-hyp scheme	414	936	374	181	118	143	230
Marquina and Mulet	414	943	373	176	111	153	229
Percentage error	0	0.8	−0.3	−2.8	−5.9	7.0	−0.4
Haas and Sturtevant	410	900	393	170	113	145	230
Percentage error	−1.0	−3.9	5.1	−6.1	−4.2	1.4	0

gas, the system is augmented with a fifth conserved variable, here the mass-fraction ϕ. The complete model is described in detail in Reference [9]:

$$U_t + F(U)_x + G(U)_y = 0, \quad U = (\rho, \rho u, \rho v, E, \rho\phi)^{\mathrm{T}}$$

$$F(U) = (\rho u, \rho u^2 + P, \rho uv, (E+P)u, \rho\phi u)^{\mathrm{T}}, \quad G(U) = (\rho v, \rho uv, \rho v^2 + P, (E+P)v, \rho\phi v)^{\mathrm{T}}$$

The ratio of specific heats of the mixture of gases is

$$\gamma(\phi) = \frac{Cp_1\phi + Cp_2(1-\phi)}{Cv_1\phi + Cv_2(1-\phi)}$$

and the equation of state reads $P = (\gamma(\phi) - 1)(E - \rho(u^2 + v^2)/2$.

Given this formulation in conservation form, finite volume methods as described above are applicable provided a splitting of the flux $(F, G)^{\mathrm{T}}$ is available. Like in Reference [9] we apply Marquina's splitting from Reference [10]. The bi-hyperbolic reconstruction resolves the flow quite well. In Table I we display the velocities for certain flow features such as the speed of the shock waves (V_s: incident shock, V_r: refracted shock, V_t; transmitted shock), the interface of the bubble (V_{ui}, V_{di}: upstream resp. downstream border of the bubble) and the air jet head (V_j). Notations are taken from Reference [9], where more details can be found.

The results are well within the estimated error bounds of 10% for the experiment [8] and we note the close agreement with the numerical results from Marquina and Mulet [9], although their results are obtained from a fifth-order WENO scheme on a grid of 8000×800 points compared to our third-order method on 3000×300 points. Still, the bi-hyperbolic reconstruction prescribes enough numerical viscosity to avoid pressure fluctuations at the interfaces between the regions of different gases, a well-known problem for conservative schemes.

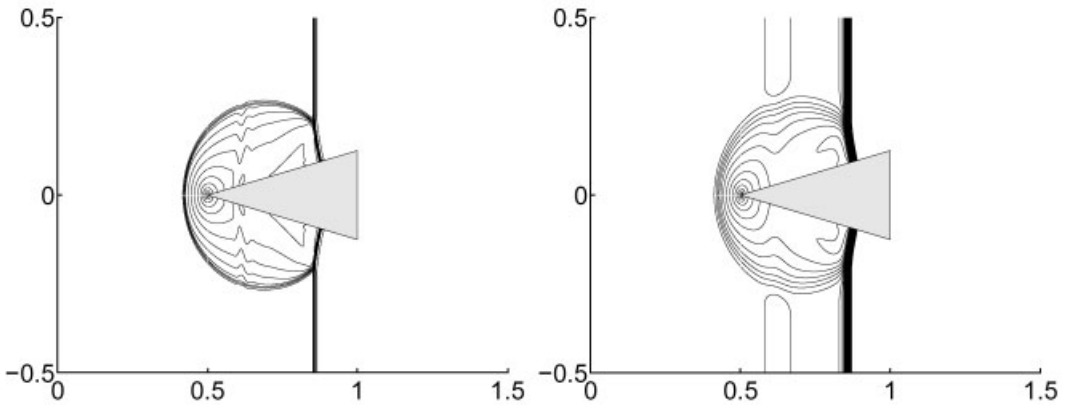

Figure 3. Density contours at $t = 0.26$ s with and without reconstruction.

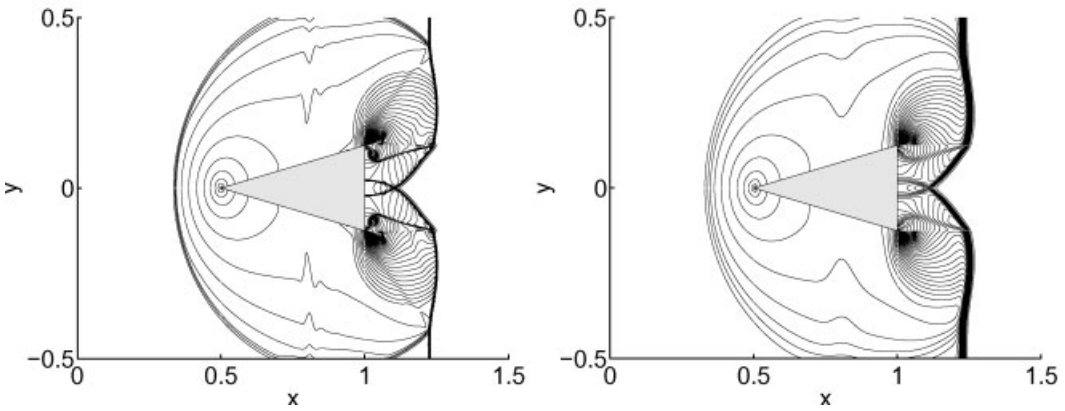

Figure 4. Density contours at $t = 0.45$ s with and without reconstruction.

Triangular obstacle

A strong air shock wave travels against a reflective triangular obstacle; see Figures 3 and 4. Due to the geometry of the domain, it is suitable to use non-Cartesian cells around the triangle. Simulations both with and without reconstructions are compared, and one sees a clear improvement in the resolution for the simulation using bi-hyperbolic reconstruction. Both simulations have been performed on parallel computers using 130 000 grid cells.

ACKNOWLEDGEMENTS

Support by the European network HYKE, funded by the EC as contract HPRN-CT-2002-00282, is acknowledged.

REFERENCES

1. Marquina A. Local piecewise hyperbolic reconstruction of numerical fluxes for nonlinear scalar conservation laws. *SIAM Journal on Scientific Computing* **15**(4):892–915.
2. Schroll HJ, Svensson F. A bi-hyperbolic finite volume method on curvilinear meshes. *Journal of Scientific Computing*, to appear.
3. Schroll HJ. High resolution schemes for hyperbolic conservation laws. *Journal of Scientific Computing* 2004; **21**(2):251–279.
4. Donat R, Marquina A. Capturing shock reflections: an improved flux formula. *Journal on Computational Physics* 1996; **125**:42–58.
5. Li S, Petzold L. Moving mesh methods with upwinding schemes for timedependent PDEs. *Journal on Computational Physics* 1997; **131**:368–377.
6. van Leer B. In *Flux-Vector Splitting for the Euler Equations*, Krause E (ed.), Lecture Notes in Physics. Springer: Berlin, 1982; **170**:507.
7. Gottlieb S, Shu CW, Tadmor E. Strong stability-preserving high order time discretization methods. *SIAM Review* 2001; **43**:89–112.
8. Haas J-F, Sturtevant B. Interaction of weak shock waves with cylindrical and spherical gas inhomogeneities. *Journal of Fluid Mechanics* 1987; **181**:41–76.
9. Marquina A, Mulet P. A flux split algorithm applied to conservative models for multicomponent compressible flows. *Journal on Computational Physics* 2003; **185**:120–138.
10. Donat R, Marquina A. Capturing shock reflections: an improved flux formula. *Journal on Computational Physics* 1996; **125**:42–58.
11. Shu CW. Essentially non-oscillatory and weighted essentially non-oscillatory schemes for hyperbolic conservation laws. In *Advanced Numerical Approximation of Nonlinear Hyperbolic Equations*, Quateroni A (ed.), Lecture Notes in Mathematics. Springer: Berlin, 1998; 325–432.
12. Artebrant R, Schroll J. Conservative logarithmic reconstructions and finite volume methods. *SIAM Journal on Scientific Computing*, to appear.

